

Spatial control of the competition between self-focusing and self-defocusing nonlinearities in one- and two-dimensional systems

Nguyen Viet Hung¹, Marek Trippenbach², Eryk Infeld³, and Boris A. Malomed⁴

¹*Advanced Institute for Science and Technology (AIST),
Hanoi University of Science and Technology (HUST), Hanoi, Vietnam*

²*Institute of Theoretical Physics, Physics Department,
Warsaw University, Hoża 69, PL-00-681 Warsaw, Poland*

³*National Centre for Nuclear Research, Hoża 69, PL-00-681 Warsaw, Poland and*

⁴*Department of Physical Electronics, School of Electrical Engineering,
Faculty of Engineering, Tel Aviv University, Tel Aviv 69978, Israel*

We introduce a system with competing self-focusing (SF) and self-defocusing (SDF) terms, which have the same scaling dimension. In the one-dimensional (1D) system, this setting is provided by a combination of the SF cubic term multiplied by the delta-function, $\delta(x)$, and a spatially uniform SDF quintic term. This system gives rise to the most general family of *1D Townes solitons*, the entire family being unstable. However, it is completely stabilized by a finite-width regularization of the δ -function. The results are produced by means of numerical and analytical methods. We also consider the system with a symmetric pair of regularized δ -functions, which gives rise to a wealth of symmetric, antisymmetric, and asymmetric solitons, linked by a bifurcation loop, that accounts for the breaking and restoration of the symmetry. Soliton families in 2D versions of both the single- and double-delta-functional systems are also studied. The 1D and 2D settings may be realized for spatial solitons in optics, and in Bose-Einstein condensates.

I. INTRODUCTION

The creation of various self-trapped modes (loosely called “solitons” in this paper) in many physical systems is complicated by competition between self-focusing (SF) and self-defocusing (SDF) nonlinearities. The first example, which was studied in detail, is the competition between the second-harmonic-generating, i.e., quadratic, and cubic nonlinearities in optics. In such systems, the adjustment of the mismatch between the fundamental and second harmonics makes it possible to render the quadratic nonlinearity effectively self-focusing, while the cubic term may be self-defocusing. The interplay of these competing interactions gives rise to diverse soliton states, both one- and two-dimensional (1D and 2D) [1, 2].

Furthermore, a subject of many works was the competition between cubic SF and quintic SDF terms. The cubic-quintic (CQ) nonlinearity – usually, with opposite signs of the two terms – occurs in the various photonic media. Known examples include the light propagation in diverse fluids [3], specialty glasses [4], ferroelectric films [5], and colloidal suspensions of metallic nanoparticles [6]. The colloids offer remarkable flexibility, making it possible to adjust parameters of the CQ nonlinearity (the signs and magnitudes of both the cubic and quintic terms) through the selection of the diameter of the nanoparticles and the filling factor of the suspension.

The realization of the CQ nonlinearity was also theoretically elaborated in terms of the Gross-Pitaevskii equation [8] for Bose-Einstein condensates (BEC), where the quintic term accounts for three-body collisions, provided that inelastic effects may be neglected [9]. In this context, the adjustment of the nonlinearity may be provided by the Feshbach resonance which affects the sign and strength of the cubic term [10].

It has been theoretically demonstrated that the use of the CQ nonlinearity combining the SF and SDF terms opens a way to the creation of stable multidimensional solitons, including 2D [14] and 3D [11] self-trapped vortices, see a review in Ref. [12]. Recently, 2D fundamental solitons of this type were produced experimentally in colloidal waveguides [7]. The use of the CQ nonlinearity is necessary for this purpose, because the SF cubic interaction can create only the family of *Townes’ solitons* in the 2D setting, which is fully destabilized by the occurrence of the critical collapse in the same geometry [13]. The Townes’ family is degenerate, in the sense that the norm (total power) of the solitons takes the single value, which does not depend on the propagation constant. However, the 2D system including the SDF quintic term suppresses the collapse and thus lends stability to the self-trapped states, with both the fundamental and vortical internal structure [12, 14].

A degenerate family the Townes-like solitons, subject to the instability driven by the critical collapse, is known in the 1D setting as well. It is described by the nonlinear Schrödinger (NLS) equation with the quintic SF term, in the absence of cubic ones [15]. The addition of the SF cubic nonlinearity does not eliminate the collapse, but it lifts the degeneracy and stabilizes all the solitons against small perturbations [16]. It is well known too that, while the 1D NLS equation with the CQ combination of nonlinear terms is not integrable, it admits an exact analytical solutions for the full soliton family [17].

A remarkable peculiarity of the 1D NLS equation is that it admits another type of the nonlinearity, which gives rise to another degenerate soliton family, that may also be considered as a variety of the Townes' solitons. This equation contains the SF cubic nonlinear term concentrated, in the ideal form, at a single spatial point, $x = 0$, i.e., multiplied by Dirac's delta-function, $\delta(x)$. This model was introduced in Ref. [18], and it was later shown that the entire family of the solitons, whose norm does not depend on the propagation constant either (the characteristic feature of solitons of the Townes' type), is completely unstable [19]. Lifting of the degeneracy, and partial or complete stabilization of the latter family is possible in the system with two δ -functions [20, 21], or if the ideal δ -function is replaced by its finite-width counterpart [19].

The fact that two different nonlinear terms in the 1D NLS equation, $\delta(x)|U|^2U$ and $|U|^4U$, where $U(x)$ is the complex wave field, give rise to Townes-like soliton families is a unique feature of the 1D setting, which is explained by the coinciding *scaling dimension* of both these terms. This circumstance suggests to consider a general family of the Townes' solitons, produced by the 1D NLS equation including both terms. In this work, we demonstrate that such a family can be found in an exact form, and it remains degenerate (with the norm independent of the propagation constant), hence it is unstable too. In fact, another situation is more interesting, which is the main subject of the present work, *viz.*, the competition between such cubic SF and quintic SDF terms, which still share the identical scaling dimension. This situation is relevant to both physical settings mentioned above: in optical waveguides, the local cubic nonlinearity may be induced by means of locally implanted resonant dopants [22], while in BEC it can be implemented by means of the Feshbach resonance imposed by a tightly focused laser beam [23].

The most interesting issue to be considered in the framework of these systems is the stability of solitons. We conclude that, in the case of the ideal Dirac's δ -function multiplying the SF cubic term, the soliton family can be found in an exact analytical form, remaining degenerate and unstable. However, the regularization, which replaces the ideal δ -function by an approximation with a finite intrinsic scale, immediately stabilizes the entire family. This result, which is meaningful in terms of the above-mentioned physical realizations, as any locally induced nonlinearity has a finite spatial size, is obtained below by means of a combination of numerical and analytical methods. Interestingly, parts of the soliton families for which the SF or SDF term is the dominant one, turn out to be stable, severally, in accordance with the *Vakhitov-Kolokolov* (VK) criterion [13, 24] or the *anti-VK* one [25, 27]. As concerns analytical methods, we use the perturbation theory, the Thomas-Fermi approximation (TFA), and also produce particular exact solutions in the model with the regularized δ -function. Using numerical methods, we subsequently extend the analysis to the system with two regularized δ -functions, and, finally, to the 2D version of the model, with both the single and double regularized δ -functions.

The rest of the paper is organized as follows. The 1D system is formulated in Section II, where we present the basic equations and analytical solutions. Numerical and additional analytical results for the 1D systems, with the single and double regularized δ -functions, are reported in Section III. The 2D systems are introduced in Section IV, where numerical results are reported for them too. The paper is concluded by Section IV.

II. ONE-DIMENSIONAL MODELS

A. Basic equations and solutions

We start by considering the 1D NLS equation which includes competing SF cubic and SDF quintic terms:

$$iU_z = -\frac{1}{2}U_{xx} - \delta(x)|U|^2U + \sigma|U|^4U, \quad (1)$$

where constant σ is positive in the case of the competing SF-SDF nonlinearities, and $\delta(x)$ is Dirac's δ -function. It imposes a condition for the jump of the first derivative at $x = 0$:

$$U_x(x = +0) - U_x(x = -0) = -2|U(x = 0)|^2U(x = 0), \quad (2)$$

while function $U(x)$ itself is continuous at this point. Note that, although Eq. (1) admits the invariance with respect to the scaling transformation,

$$z \equiv x_0^2 \tilde{z}, \quad x \equiv x_0 \tilde{x}, \quad U \equiv x_0^{-1/2} \tilde{U}, \quad (3)$$

with arbitrary factor x_0 , it cannot alter coefficient σ in front of the quintic term, due to the above-mentioned fact that both nonlinear terms in Eq. (1) have the same scaling dimension. The presence of the *irreducible* parameter σ is an essential peculiarity of the system.

In the absence of the SDF quintic term ($\sigma = 0$), Eq. (1) has an exact stationary solution with arbitrary propagation constant $\mu > 0$, in the form of a soliton pinned to the δ -function [18, 19]:

$$U(x, z) \equiv U(x)e^{i\mu z} = (2\mu)^{1/4}e^{-\sqrt{2\mu}|x|+i\mu z}. \quad (4)$$

The total power (norm) of this pinned state is

$$N = \int_{-\infty}^{+\infty} |U(x)|^2 dx = 1, \quad (5)$$

which is independent of the propagation constant, μ [note that the norm is invariant with respect to transformation (3)]. According to the VK criterion, which states that inequality

$$dN/d\mu > 0 \quad (6)$$

is a necessary stability condition for solitons supported by a SF nonlinearity [13, 24], all solutions (4) might be neutrally stable, but in fact they all are unstable [19].

In the presence of the SDF quintic term ($\sigma > 0$), a family of exact solutions to Eq. (1) can be found in the analytical form as well:

$$U(x, z) = e^{i\mu z}U(x) = e^{i\mu z} \frac{(3\mu/\sigma)^{1/4}}{\sqrt{\sinh(\sqrt{8\mu}|x| + \xi)}}, \quad (7)$$

$$\xi = \ln \left(\sqrt{\frac{3}{2\sigma}} + \sqrt{\frac{3}{2\sigma} - 1} \right). \quad (8)$$

As follows from Eq. (8), this solution exists provided that the coefficient in front of the SDF quintic term is not too large,

$$0 < \sigma < \sigma_{\max} \equiv 3/2. \quad (9)$$

The total norm of the solution family (7) is again degenerate (it does not depend on μ , depends on σ):

$$N(\sigma) = \sqrt{\frac{3}{2\sigma}} \ln \left(\frac{\sqrt{3} + \sqrt{3-2\sigma} + \sqrt{2\sigma}}{\sqrt{3} + \sqrt{3-2\sigma} - \sqrt{2\sigma}} \right). \quad (10)$$

In particular, in the limit of $\sigma \rightarrow 0$ expression (10) continuously goes over into norm (5), $N(\sigma = 0) = 1$, while in the opposite limit of $\sigma \rightarrow \sigma_{\max}$, see Eq. (9), the norm diverges, $N \approx (1/2) \ln(1/(\sigma_{\max} - \sigma))$. In the latter limit, the peak power (squared amplitude) of the solution given by Eqs. (7) and (8) diverges too:

$$U^2(x=0) = \frac{\sqrt{3\mu/\sigma}}{\sinh \xi} \approx \sqrt{\frac{3\mu}{\sigma_{\max} - \sigma}}. \quad (11)$$

Once again, the fact that $dN/d\mu = 0$ formally suggests that the soliton family (7) might be neutrally stable according to the VK criterion, but in reality such a family of solitons with degenerate total power is *completely unstable* [19]. Thus, the combination of the cubic and quintic terms in Eq. (1) gives rise to the family of the solitons of the Townes' type (with the μ -independent norm) even in the case when the two terms are set to compete.

In the case of $\sigma < 0$ (the *cooperating*, rather than competing, nonlinearities), when both nonlinear terms in Eq. (1) have the SF sign, a family of exact soliton solutions can be readily found too:

$$U(x, z) = e^{i\mu z} \frac{(-3\mu/\sigma)^{1/4}}{\sqrt{\cosh(\sqrt{8\mu}|x| + \tilde{\xi})}}, \quad (12)$$

$$\tilde{\xi} = \ln \left(\sqrt{-\frac{3}{2\sigma}} + 1 + \sqrt{-\frac{3}{2\sigma}} \right), \quad (13)$$

cf. the exact solutions given by Eqs. (7) and (8) for the competing nonlinearities, with $\sigma > 0$. The total power of this family is

$$N(\sigma < 0) = \sqrt{-\frac{6}{\sigma}} \arctan \left(\sqrt{-\frac{3}{2\sigma}} + 1 - \sqrt{-\frac{3}{2\sigma}} \right). \quad (14)$$

Like the respective expression (10) for $\sigma > 0$, this norm does not depend on the propagation constant, μ , hence this family too is the degenerate one, of the Townes' type, and is completely unstable. However, unlike its counterpart (10), Eq. (14) demonstrates that, with the increase $-\sigma$ from zero to infinity, the total power drops from $N(\sigma \rightarrow -0) = 1$ to $N(\sigma \rightarrow -\infty) = 0$. Thus, the interplay of the cubic and quintic terms in Eq. (1) gives rise to the most general Townes-soliton family, which comprises both cases of the competing and collaborating types.

The solitons can be stabilized by a regularization of Dirac's δ -function, for which we adopt the commonly known Gaussian form:

$$\delta_{\text{Dirac}}(x) \rightarrow \delta_{\text{Gauss}}(x) \equiv (1/\sqrt{\pi}a) e^{-x^2/a^2} \quad (15)$$

with scale constant $a > 0$. Indeed, rewriting, accordingly, the corrected jump condition (2) in the form of

$$U_x(x=+0) - U_x(x=-0) = -\frac{2}{\sqrt{\pi}a} \int_{-\infty}^{+\infty} |U(x)|^2 U(x) e^{-x^2/a^2} dx, \quad (16)$$

and looking for a stationary solution to Eq. (1) with $\sigma = 0$ as $A \exp(-\sqrt{2\mu}|x| + i\mu z)$, cf. expression (4), the calculation of the integral on the right-hand side of Eq. (16) yields the first correction to the squared amplitude for small a (or for small μ , if $a = 1$ is fixed, see below),

$$A^2 \approx \sqrt{2\mu} \left(1 + 3\sqrt{2\mu/\pi}a\right), \quad (17)$$

and the respective correction to norm (5),

$$N \approx \left(1 + 3\sqrt{2\mu/\pi}a\right), \quad (18)$$

which satisfies the VK criterion (6). The consistent stability analysis for the model with the δ -function regularized as per Eq. (15) is developed below in a numerical form.

To further illustrate effects of the regularization of the δ -function, it is worthy to briefly consider another functional form of the smoothing, with scale constant b :

$$\delta_{\text{Dirac}}(x) \rightarrow \delta_{\text{sech}}(x) \equiv (\pi b)^{-1} \text{sech}(x/b), \quad (19)$$

which satisfies the standard normalization condition, $\int_{-\infty}^{+\infty} \delta_{\text{sech}}(x) dx \equiv 1$. It is easy to see that Eq. (1) with the δ -function replaced by expression (19) admits two exact solutions for pinned solitons,

$$\begin{aligned} U(x, z) &= \exp(i\mu_b z) U_b \sqrt{\text{sech}\left(\frac{x}{b}\right)}, \\ \mu_b &= \frac{1}{8b^2}, \quad U_b^2 = \frac{1}{2\pi\sigma b} \left(1 \pm \sqrt{1 - \frac{3}{2}\pi^2\sigma}\right) \end{aligned} \quad (20)$$

which exists for $0 < \sigma < \tilde{\sigma}_{\text{max}} \equiv 2/(3\pi^2)$, cf. Eq. (9) [exact solution (20) with upper sign is relevant for $\sigma < 0$ too]. The total power of these solutions does not depend on scale constant b :

$$N_b^{(\pm)} = \frac{1}{2\sigma} \left(1 \pm \sqrt{1 - \frac{3}{2}\pi^2\sigma}\right). \quad (21)$$

B. The linear-stability analysis

To study the stability of solitons pinned to the effective delta-functional nonlinear potential well, we first concentrate on solutions of Eq. (1) with the δ -functions regularized as per Eq. (15). The stationary solution is taken as $U(x, z) = e^{i\mu z} U(x)$, where $U(x)$ is assumed real, with propagation constant $\mu > 0$. A small perturbation is added to the solution in the form of

$$\tilde{U}(x, z) = [U(x) + \delta u(x, z)] e^{i\mu z} \quad (22)$$

with $|\delta u(x, z)| \ll |U(x)|$. Substituting this into Eq. (1) and linearizing, we derive the evolution equation for the perturbation,

$$i(\delta u)_z = -\frac{1}{2}(\delta u)_{xx} + [3\sigma U^4(x) - 2\delta(x)U^2(x) + \mu]\delta u + U^2(x)[2\sigma U^2(x) - \delta(x)]\delta u^*. \quad (23)$$

We rewrite this equation in matrix form,

$$i \begin{pmatrix} (\delta u)_z \\ (\delta u^*)_z \end{pmatrix} = \begin{pmatrix} \hat{A} & \hat{B} \\ -\hat{B} & -\hat{A} \end{pmatrix} \begin{pmatrix} \delta u \\ \delta u^* \end{pmatrix} \quad (24)$$

$$\hat{A} \equiv -(1/2)\partial_{xx} + 3\sigma U(x)^4 - 2\delta(x)U(x)^2 + \mu, \quad (25)$$

$$\hat{B} \equiv 2\sigma U(x)^4 - \delta(x)U(x)^2. \quad (26)$$

Eigenfunctions of perturbation $\delta u(x, z)$ are looked for in the form of

$$\delta u(x, z) = f(x)e^{\lambda z} + g^*(x)e^{\lambda^* z} \quad (27)$$

where λ is a complex stability eigenvalue, and $\{f(x), g(x)\}$ are respective complex eigenfunctions. The substitution of perturbation (27) into Eq. (24) leads to the following eigenvalue problem,

$$i \begin{pmatrix} 0 & \hat{C} \\ \hat{D} & 0 \end{pmatrix} \begin{pmatrix} \eta \\ \chi \end{pmatrix} = \lambda \begin{pmatrix} \chi \\ \eta \end{pmatrix}. \quad (28)$$

Here $\eta \equiv f(x) + g(x)$, $\chi \equiv f(x) - g(x)$, and $\hat{C} \equiv \hat{A} + \hat{B}$, $\hat{D} \equiv \hat{A} - \hat{B}$. Equation (28) was solved numerically. Obviously, the soliton is unstable if there is at least one eigenvalue with $\lambda_r > 0$. Alternatively, the stability of the soliton can be tested in direct simulations, in which the perturbations are applied to initial conditions for Eqs. (1) and (29). In the next section, we use both methods.

C. The double-delta structure

Next, we consider the model with two identical delta-functions,

$$iU_z = -\frac{1}{2}U_{xx} - [\delta(x-1) + \delta(x+1)]|U|^2U + \sigma|U|^4U, \quad (29)$$

where coefficient $\sigma \geq 0$ remains irreducible, while the distance between the δ -functions may be set equal to 2 by means of rescaling (3). Exact analytical solutions to Eq. (29) with $\sigma = 0$ were found for symmetric, antisymmetric, and asymmetric solitons pinned to the two δ -functions [20], the asymmetry parameter being defined as

$$\nu = N^{-1} \left[\int_0^{+\infty} |U(x)|^2 dx - \int_{-\infty}^0 |U(x)|^2 dx \right]. \quad (30)$$

In the case of $\sigma = 0$, the symmetric solitons are completely stable, while the antisymmetric and asymmetric ones are completely unstable. Stabilization of the asymmetric and antisymmetric solitons is possible, as shown in Ref. [20], by replacing each ideal δ -functions with its regularized version, as per Eq. (15).

D. Rescaling of the parameters

The rescaling transformation (3) applies as well to Eqs. (1) and (29) in which the δ -function is replaced by its regularized version (15). We use this degree of freedom to fix the regularization spatial scale as $a \equiv 1$, thus replacing Eq. (1) by

$$iU_z = -\frac{1}{2}U_{xx} - \frac{e^{-x^2}}{\sqrt{\pi}}|U|^2U + \sigma|U|^4U. \quad (31)$$

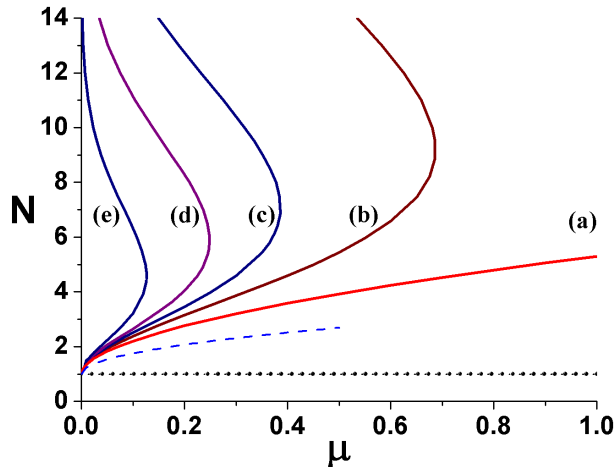


FIG. 1: (Color online) Families of numerically found stationary soliton solutions to Eq. (31) for the 1D single-well configuration. The dependence of the total power on the propagation constant, $N(\mu)$, is shown for several values of the quintic coefficient: (a) $\sigma = 0$, (b) $\sigma = 0.05$, (c) $\sigma = 0.075$, (d) $\sigma = 0.1$ and (e) $\sigma = 0.15$. All these curves represent *stable solitons*. The dashed curve shows analytical approximation (18) for $\sigma = 0$. The horizontal dotted line corresponds to $N(\mu) \equiv 1$, $\sigma = 0$. The latter family, given by Eqs. (7) and (8), is unstable. Qualitatively, the shape of the $N(\mu)$ curves in this figure is explained by the Thomas-Fermi approximation based on Eqs. (35)-(37).

In the model with the double δ -function, we again fix $a = 1$, hence the distance between the two attraction centers is no longer 2 [see Eq. (29)], but becomes an independent parameter, $2x_0$. Thus, the regularized version of Eq. (29) is

$$iU_z = -\frac{1}{2}U_{xx} - \frac{1}{\sqrt{\pi}} \left[e^{-(x-x_0)^2} + e^{-(x+x_0)^2} \right] |U|^2 U + \sigma |U|^4 U. \quad (32)$$

It is easy to check that the function multiplying the SF cubic term in Eq. (32) keeps the double-well structure at

$$x_0 > (x_0)_{\min} = 1/\sqrt{2}. \quad (33)$$

III. NUMERICAL AND ANALYTICAL RESULTS FOR THE ONE-DIMENSIONAL SYSTEMS

In our numerical calculations, we chiefly used the imaginary-time-propagation method for finding stationary solutions, and the split-step Fourier algorithm for simulations of their perturbed evolution. To obtain antisymmetric structures, we have additionally used the Newton conjugate gradient method [29, 30]. The linear eigenvalue problem represented by Eq. (28) was solved by means of the Fourier collocation method.

A. The single-well setting: numerical results

First, we address soliton solutions generated by Eq. (1) with the δ -function regularized as per Eq. (15), expecting the stabilization of these states – at least, for small μ , according to the analytical result (18), which satisfies the VK criterion. The setting is fully characterized by two independent parameters, σ and N . The summary of the results is presented in Fig. 1.

A salient feature of Fig. 1 is the presence of upper and lower branches in dependences $N(\mu)$, connected at the rightmost turning point. To highlight the difference between solitons pertaining to the same value of μ but lying on the upper and lower branches, in Fig. 2 we display profiles of such a pair of solitons with strongly differing values of the total power.

The numerical analysis, including both the computation of eigenvalues for small perturbations on the basis of Eq. (24) and direct simulations, demonstrates that *all* the 1D solitons trapped in the single-well nonlinear potential are indeed *stable* if the Gaussian regularization (15) is used instead of the ideal δ -function. In particular, the stability of

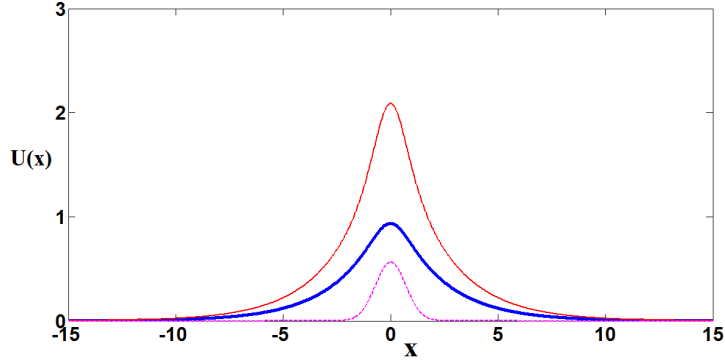


FIG. 2: (Color online) The thin upper and bold intermediate curves show an example of a pair of stable 1D solitons pinned to the single regularized δ -function, in the model with $\sigma = 0.1$. The dashed bottom curve depicts profile (15) of the regularized δ -function. These solitons pertain to a common value of the propagation constant, $\mu = 0.1$, while their total powers (norms) are $N_1 = 11.16$ and $N_2 = 2.66$, respectively.

the solution branch with $\sigma = 0$ in Fig. 1, which is produced by the SF-only nonlinearity, complies with the evident fact that this branch satisfies the VK criterion. As concerns the branches for $\sigma > 0$, their stability for relatively small values of N , beneath the turning points, where the SF term dominates, may also be explained by the VK criterion. On the other hand, above the turning points, where, due to large values of N , the SDF term is the dominant one, the stability agrees with the anti-VK criterion, $dN/d\mu < 0$, which applies to solitons supported by the SDF nonlinearity [25]. In fact, such an effective switch between the VK and anti-VK criteria at a turning point, which secures the stability of the entire soliton branch, occurs in other systems featuring the competition between SF and SDF terms [31].

Dependences $N(\sigma)$ for different values of μ are displayed in Fig. 3(a), and compared to the dependence given by Eq. (10), which was obtained in the exact form for the ideal δ -function, and which does not depend on μ . As seen in the figure, the largest value of the quintic SDF coefficient, σ_{cr} , up to which the solitons exist in the system, is close to absolute maximum, $\sigma_{\text{max}} = 3/2$, given by Eq. (9), for small μ , at which there are broad solitons similar to those supported by the ideal δ -function (but are stable, on the contrary to that case). With the increase of μ , the solitons become narrower, and σ_{cr} decreases, so that there appears the dependence between N and σ_{cr} displayed in Fig. 3(b).

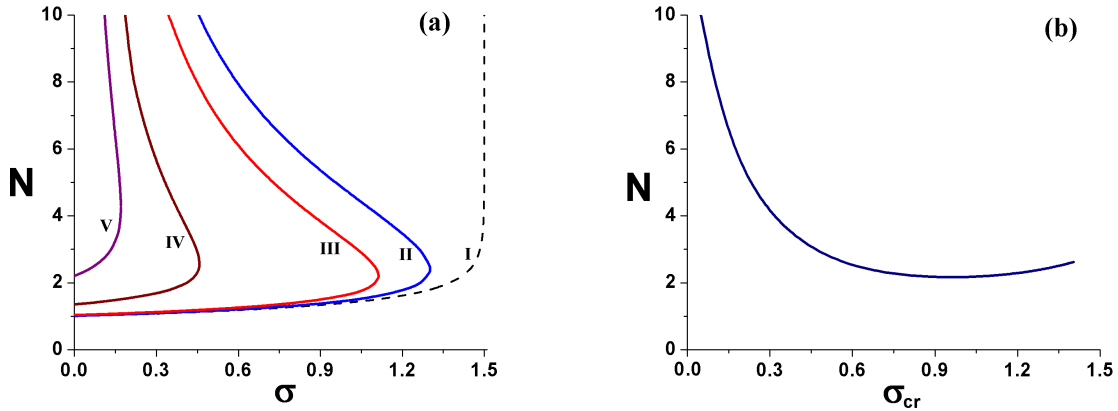


FIG. 3: (Color online) (a) Dependences $N(\sigma)$ for soliton families produced by equation (31) with $\mu = 10^{-1}$ (curve V), $\mu = 10^{-2}$ (curve IV), $\mu = 10^{-4}$ (curve III), and $\mu = 10^{-5}$ (curve II). The dashed curve I represents the exact result (10) obtained with the ideal δ -function (in this case, N does not depend μ). (b) Dependence $N(\sigma_{\text{cr}})$, where σ_{cr} is the largest value of the quintic coefficient, σ , at which the solitons exist in (a).

B. The single-well setting: analytical results

The shape of the $N(\sigma)$ curves in Fig. 3(a), i.e., the fact that, at small σ , one has two solitons corresponding to a common value of μ , one with the total power N close to 1, and another one with apparently larger N , can be explained by the particular exact solutions given by Eqs. (19)-(21). Indeed, both solutions pertain to the common propagation constant, $\mu_b = 1/(8b^2)$, and, at small σ , one has a moderate value of the power, $N_b^{(-)} \approx 3\pi^2/8$, while the other features a large power,

$$N_b^{(+)} \approx 1/\sigma. \quad (34)$$

Another qualitative explanation for the existence of the upper and lower solution branches in Fig. 3(a) is offered by the Thomas-Fermi approximation (TFA), which is an efficient method for describing the shape of solitons supported by the SDF nonlinearity [32, 33]. In its simplest form, the TFA neglects the second derivative in Eq. (31). For given $\mu > 0$, this approximation yields a *pair* of localized solutions, which may be interpreted as those representing the upper and lower branches in Fig. 3(a):

$$U(x, z) = \frac{1}{\sqrt{2\sqrt{\pi}\sigma}} e^{i\mu z} \begin{cases} \sqrt{\exp(-x^2) \pm \sqrt{\exp(-2x^2) - 4\pi\sigma\mu}}, & \text{at } |x| \leq x_0 \equiv \sqrt{-\frac{1}{2} \ln(4\pi\sigma\mu)}, \\ \exp[-x_0^2/2 - \sqrt{2\mu}(|x| - x_0)], & \text{at } |x| > x_0. \end{cases} \quad (35)$$

The second line in Eq. (35) represents spatially decaying tails, attached to the TFA-predicted core part of the soliton. The tails are produced by the linearized version of Eq. (31), where the second derivative is kept, cf. a similar combined approximation developed for gap solitons in Ref. [33]. The TFA given by Eq. (35) is valid under the condition that the expression under the square root is positive at $x = 0$, i.e., at

$$\mu < \mu_{\max}^{(\text{TFA})} \equiv (4\pi\sigma)^{-1}. \quad (36)$$

The latter condition offers a qualitative explanation to the existence of the turning points in Fig. 3(a). Further, the TFA makes it possible to find the asymptotic value of the total power corresponding to the upper branches of $N(\mu)$ in the figure:

$$\lim_{\mu \rightarrow 0} \{N(\mu; \sigma)\}_{\text{TFA}} = 1/\sigma, \quad (37)$$

which, incidentally, agrees with Eq. (34). An essential corollary of Eq. (37) is the fact that $N(\mu)$ remains finite (does not diverge) at $\mu \rightarrow 0$ along the upper branches in Fig. 3(a).

C. The double-well setting

The double-well configuration based on Eq. (32) is controlled by three parameters, x_0 , σ and N . In the limit of $\sigma \rightarrow 0$ (no SDF quintic term), this system turns into the one considered in Ref. [20] (a similar system with a two-component field, which demonstrates an extremely complex picture of transitions between symmetric, antisymmetric, and antisymmetric states, was considered in Ref. [21]). Therefore, we started the numerical analysis of the double-well setting with small values of σ , aiming to produce new results at larger σ .

In the simulations, symmetric and asymmetric states, with the symmetry defined with respect to the two identical nonlinear-potential wells, were generated using the initial guess

$$\{u(x)\}_{\text{sym,asym}}^{(\text{in})} = P \operatorname{sech}(x + x_0) + Q \operatorname{sech}(x - x_0), \quad (38)$$

with constants $P = Q$ and $P \neq Q$ for the symmetric and asymmetric ones. Antisymmetric states were created starting from the input

$$\{u(x)\}_{\text{antisym}}^{(\text{in})} = P \operatorname{sech}(qx) \sin(kx), \quad (39)$$

with some constants q and k .

We start by presenting, in Fig. 4, examples of stable unstable symmetric solitons, As shown in this figure, unstable symmetric solitons spontaneously transform themselves into asymmetric breathers trapped in a single well. Further, examples of stable and unstable antisymmetric solitons are displayed in Fig. 5. It is seen that even a weak SDF term (with $\sigma = 0.01$) is able to stabilize the antisymmetric soliton, while an unstable one spontaneously transforms

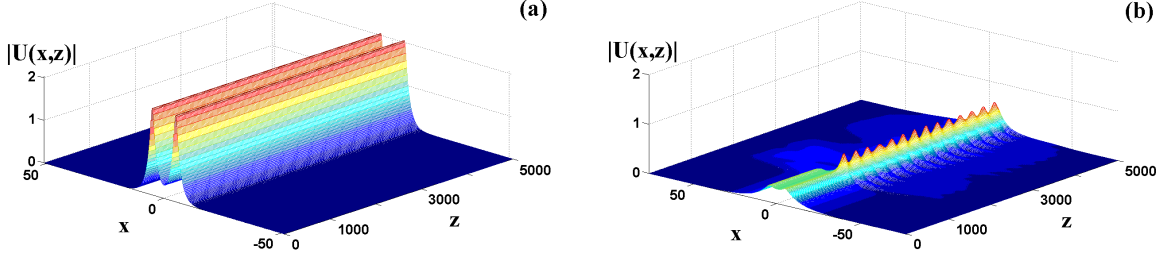


FIG. 4: (Color online) Examples of the evolution of stable and unstable symmetric solitons in the 1D double-well model, for $x_0 = 5$, $\sigma = 0.1$, $\mu = 0.14$, and $x_0 = 5$, $\sigma = 0.05$, $\mu = 0.008$, respectively.

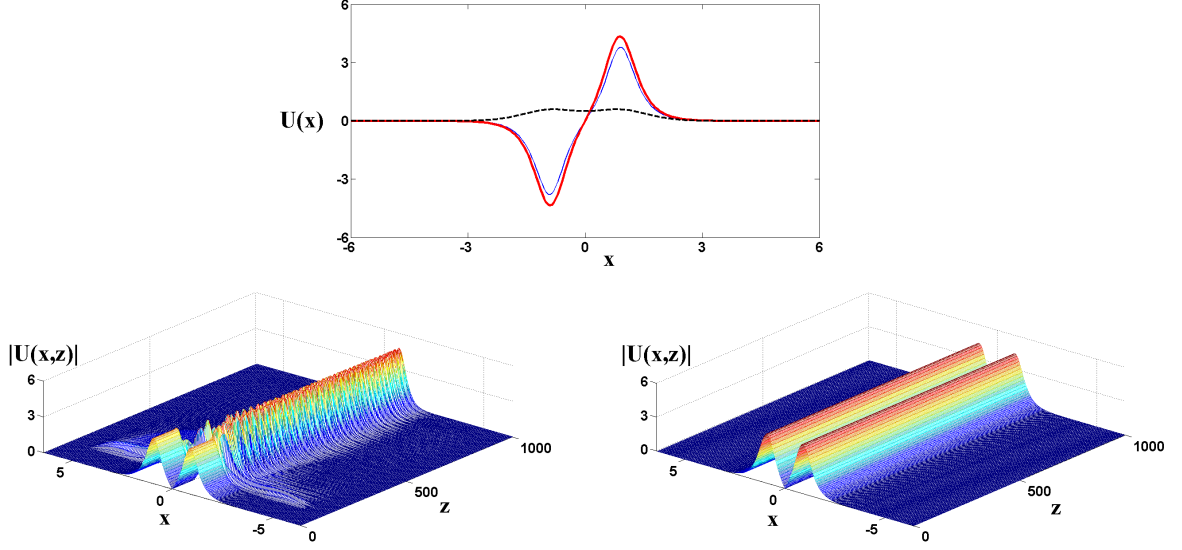


FIG. 5: (Color online) A stable antisymmetric soliton with norm $N = 26.394$ (the bold curve in the top frame, and the right frame below) produced by Eq. (29) with $\sigma = 0.01$, compared to an unstable antisymmetric one with $N = 18.816$ (the thin curve in the top frame, and the left frame below) obtained, as in Ref. [20], for $\sigma = 0$. The other parameters are: $x_0 = 0.9$ (the dashed curve in the top frame depicts profile of the cubic nonlinear regularization in the equation (32)), $\mu = 3.8688$ [cf. Fig. 8(b) in Ref. [20]].

into a nearly stationary strongly asymmetric state, trapped in a single well. Asymmetric solitons may also be stable or unstable, as shown in Fig. 6, the unstable one transforming into a breather which stays trapped in the original nonlinear-potential well.

Families of stable and unstable symmetric, antisymmetric, and asymmetric solitons are linked into a rather complex bifurcation diagram, which is presented in Fig. 7. The lower panel of the figure demonstrates that the asymmetric soliton family branches out from the symmetric one at a very small value of the total power, $N \approx 1.3$, and then it disappears at $N \approx 19$, merging into a common turning point of the symmetric and antisymmetric branches. Further, it is worthy to note that the stability of the symmetric and antisymmetric families obeys the anti-VK and VK criteria, respectively, while the asymmetric branches may feature either type of the stability.

Another adequate picture of the set of soliton families in the double-well system is provided by the symmetry-breaking bifurcation diagram which is displayed in Fig. 8. A characteristic feature of this picture is the loop connecting the symmetry-breaking and symmetry-restoring bifurcations. A similar feature was earlier found in dual-core systems carrying spatially uniform competing SF cubic and SDF quintic nonlinearities [34]. Note that the loop shown in Fig. 8 has a concave shape. For a stronger coupling between the two wells, which corresponds to smaller values of x_0 , it is expected that the loop will shrink and acquire a convex form, cf. the loops in the 2D model displayed below in Figs. 19 and 22. Eventually, the loop will disappear at still smaller x_0 [34].

The results are finally summarized in Fig. 9, which displays stability domains for the symmetric, antisymmetric, and

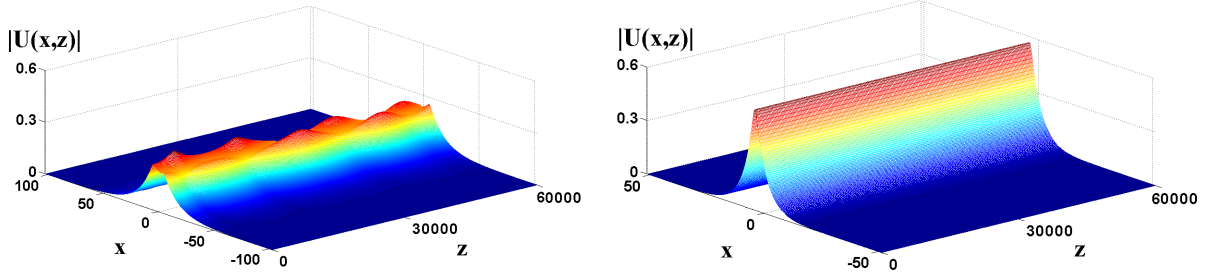


FIG. 6: (Color online) Evolution of unstable ($x_0 = 5$, $\sigma = 0.2$, $\mu = 0.003$) and stable ($x_0 = 4$, $\sigma = 0.1$, $\mu = 0.025$) asymmetric solitons in the 1D double-well model.

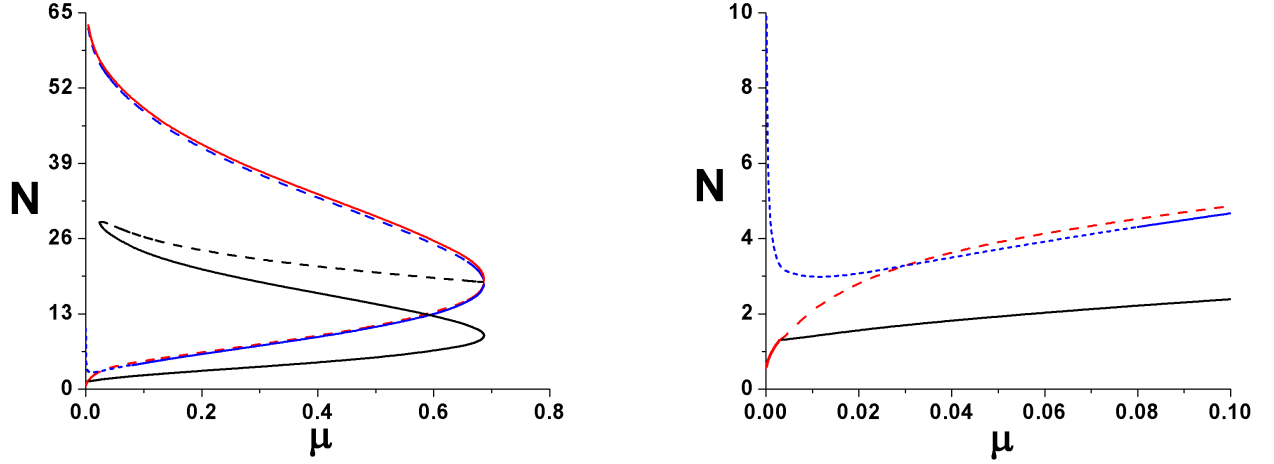


FIG. 7: (Color online) The bifurcation diagram for the 1D double-well system, shown in terms of $N(\mu)$ curves, for $x_0 = 5$ and $\sigma = 0.05$ (the left panel), and the closeup of the symmetry-breaking part for smaller values of μ (the right panel). Here and in the next figure, red, blue, and black curves represent symmetric, antisymmetric, and asymmetric modes, respectively, while solid and dashed segments of the curves refer to stable and unstable solitons.

asymmetric solitons, in the plane of the quintic SDF coefficient, σ , and the total norm, N . The figure demonstrates that the stability areas for the antisymmetric and asymmetric model shrink with the increase of the SDF coefficient, σ , as well as with the decrease of the distance ($2x_0$) between the two wells. The latter trend is quite natural, as at $x_0 < 1/\sqrt{2}$ [see Eq. (33)] the double-well structure turns into the single-well one, which cannot support states different from the symmetric ones. The former feature is natural too, as the increase of the SDF strength makes the modes broader, favoring the simple symmetric profiles. Note that the system exhibits bistability, in the form of the overlap between the stability regions of asymmetric solitons with those of the symmetric and antisymmetric ones.

IV. TWO-DIMENSIONAL MODELS

A. The formulation

The 1D models considered in above can be naturally extended to 2D, similar to how the 1D system with two nonlinear potential wells [20] was generalized into the 2D setting in Ref. [26]. Here we model our 2D systems by equations

$$iU_z = -\frac{1}{2}(U_{xx} + U_{yy}) - \tilde{\delta}_{2D}(x, y)|U|^2U + \sigma|U|^4U, \quad (40)$$

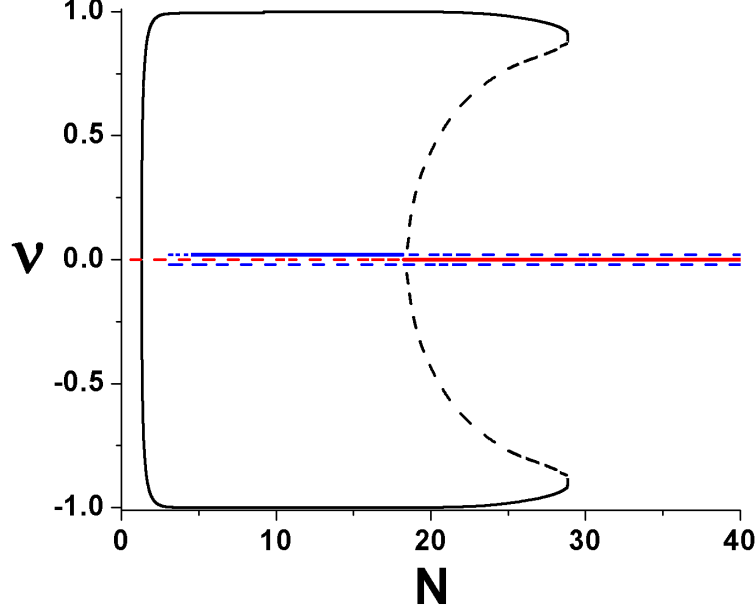


FIG. 8: (Color online) The asymmetry parameter (30) vs. total power N for the same set of soliton branches in the 1D double-well system with $x_0 = 5$ and $\sigma = 0.05$ which is shown in Fig. 7.

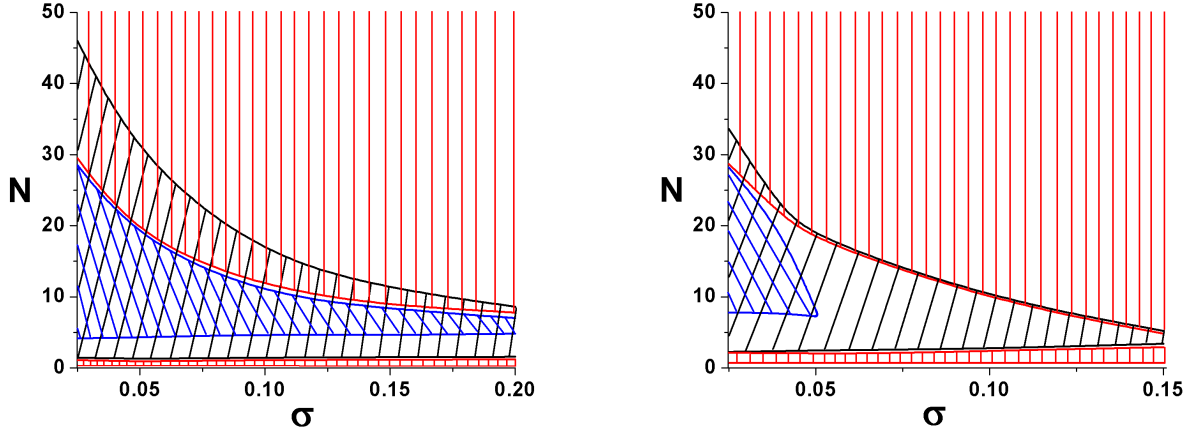


FIG. 9: (Color online) Stability areas for symmetric, antisymmetric, and asymmetric solitons (red (vertical), blue (leftward), and black (rightward), respectively) in the plane of (σ, N) in the 1D double-well system based on Eq. (29). The half-distance between the wells is, severally, $x_0 = 5$ and 1.25 in the left and right panels.

in the case of single potential well and,

$$iU_z = -\frac{1}{2}(U_{xx} + U_{yy}) - [\tilde{\delta}_{2D}(x - x_0, y) + \tilde{\delta}_{2D}(x + x_0, y)]|U|^2U + \sigma|U|^4U, \quad (41)$$

for the double-well case. The regularized 2D counterpart of the δ -function used in these equations is defined as

$$\tilde{\delta}_{2D}(x, y) = \begin{cases} (\pi a^2)^{-1}, & \text{at } x^2 + y^2 < a^2. \\ 0, & \text{at } x^2 + y^2 > a^2. \end{cases} \quad (42)$$

which satisfies the normalization condition, $\int \int \tilde{\delta}_{2D}(x, y) dx dy = 1$. By means of the rescaling, we set the regularization scale $a = 1/2$ in Eq. (42). We consider cases of the separated circles in Eq. (41), with $x_0 > 1/2$, and partly overlapping ones, with $x_0 < 1/2$. In addition to x_0 , Eq. (40) is governed by two remaining independent parameters: σ and the two-dimensional total power (norm),

$$N = \int \int |U(x, y)|^2 dx dy \quad (43)$$

(or the respective propagation constant, μ), while Eq. (41) features three parameters: σ , N (or μ) and the distance between the wells, $2x_0$. The asymmetry of 2D modes with respect to the two identical circles in Eq. (41) is defined as a counterpart of the 1D definition (30):

$$\nu = N^{-1} \int_{-\infty}^{+\infty} dy \left[\int_0^{+\infty} |U(x, y)|^2 dx - \int_{-\infty}^0 |U(x, y)|^2 dx \right]. \quad (44)$$

The 2D models were investigated only in the numerical form, as an analytical approach would be too difficult in this case. Stationary solutions were constructed by means of the Newton conjugate gradient method [29, 30]. The imaginary-time-integration method does not converge in this case, but we used intermediate states generated by it as an input for the Newton's method. The stability of the 2D states was tested by means of the split-step Fourier method in direct simulations. Results of the direct simulations were confirmed by computation of eigenvalues for small perturbations, which was carried out with the help of the Newton conjugate gradient method and the Fourier collocation method.

B. The single-well model

Figure 10 shows curves $N(\mu)$ for solitons produced by Eq. (40) for selected values of the quintic coefficient. In the bottom left panel, we show a close-up of the picture at small values of propagation constant μ , where one can observe the transition from stable to unstable solutions. In fact, curve (a), pertaining to $\sigma = 0$, reproduces the results reported in Refs. [26] and [35], with the norm of the stable solitons bounded from above by the collapse [13]. In this case, the stability of the solitons is secured by the VK criterion. In the presence of the quintic term [curves (b) - (e) in Fig. 10], additional (upper) stable soliton branches appear, which obey the anti-VK criterion, making the situation similar to that in 1D, cf. Fig. 1. Additional unstable branches, specific to the 2D setting, which do not satisfy the VK criterion, exist at small values of μ , as shown in detail in the left bottom panel of Fig. 10. In direct simulations, displayed in Fig. 11, solitons belonging to an unstable branch at first lose a part of the norm through the emission of radiation, and later transform themselves into robust breathers. As concerns the shape of the boundary of the region where stable 2D solitons exist in the right panel of Fig. 10, the necessary value of the quintic coefficient, σ , grows (roughly, linearly) with N , as the sufficiently strong SDF quintic term is necessary to stabilize the solitons against the collapse.

C. The double-well model

Extending the analysis to the 2D model with two regularized δ -functions, described by Eq. (41), we have found that the model can support stable symmetric, antisymmetric and asymmetric states, where, like in the 1D setting, the asymmetry is defined with respect to the two identical regularized δ -functions, i.e., the circles in Eq. (41). The respective asymmetry measure, ν , is defined by Eq. (44).

Typical examples of symmetric, asymmetric and antisymmetric solitons are displayed in Figs. 12 – 18. Note that symmetric solitons may feature both single-peak and double-peak shapes. In particular, unstable single-peak symmetric solitons spontaneously turn into excited asymmetric solitons, while unstable double-peak symmetric solitons radiate away a part of their norm before turning into strongly excited asymmetric solitons, see Figs. 13 and 14). A typical example of the evolution of an unstable asymmetric soliton is presented in Fig. 16, where we observe its spontaneous transformation into a robust asymmetric breather, following shedding off a part of its norm with transient radiation.

The results of the numerical analysis of the 2D double-well system are summarized in Figs. 19 - 22, which address the existence and stability, represented by curves $N(\mu)$, and the symmetry breaking between the wells, represented by the $\nu(N)$ curves, for two generic situations, which correspond to the separated circles ($x_0 > 1/2$) or partly overlapping ones ($x_0 < 1/2$). In the latter case, the $N(\mu)$ curves are similar to their counterpart in the 1D model, cf. Fig. 1. In

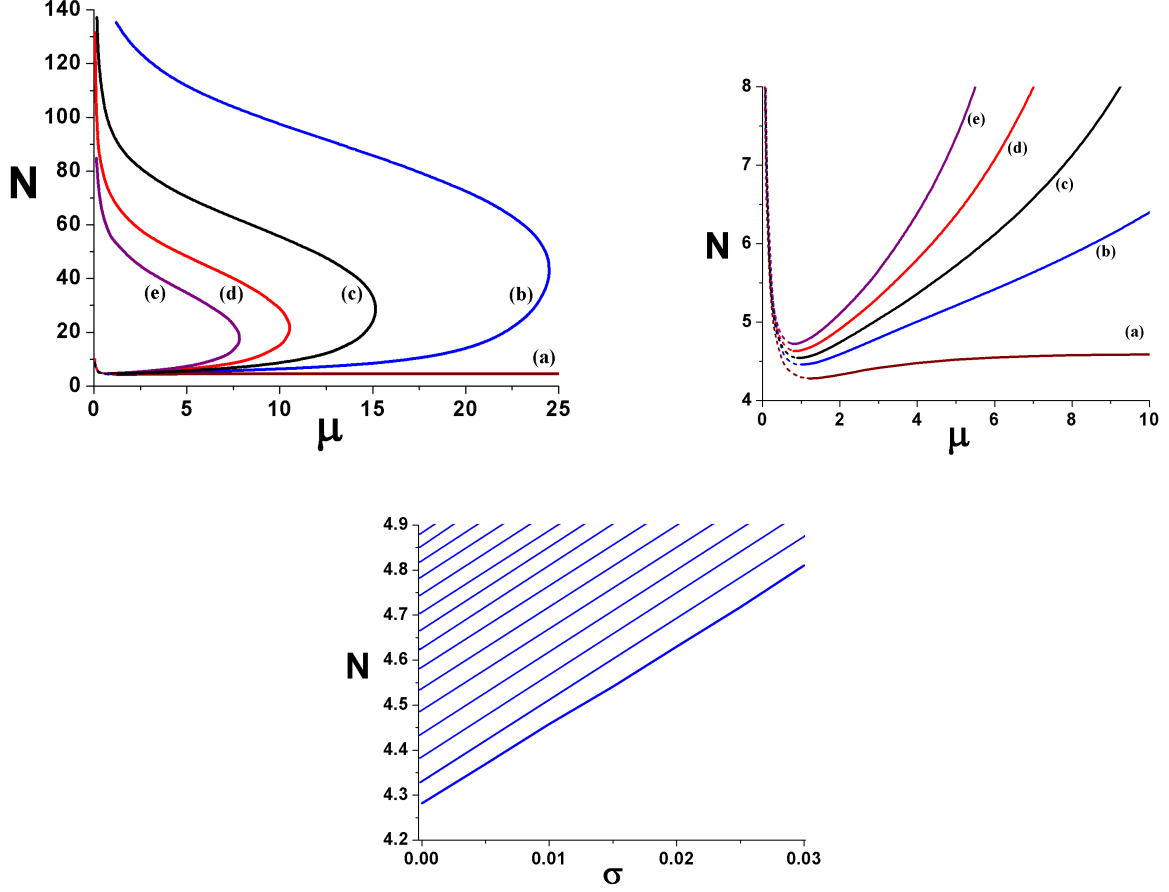


FIG. 10: (Color online) Numerical results for the 2D single-well model represented by Eq. (40). The upper panel shows a set of $N(\mu)$ curves for the following values of the SDF quintic coefficient: $\sigma = 0$ (a), $\sigma = 0.01$ (b), $\sigma = 0.015$ (c), $\sigma = 0.02$ (d) and $\sigma = 0.025$ (e). The left bottom panel shows a closeup of the region of small μ , where the transition from stable (solid) branches to unstable (dashed) ones occurs. In the right bottom panel, the domain where the system supports stable solitons is shaded by oblique lines.

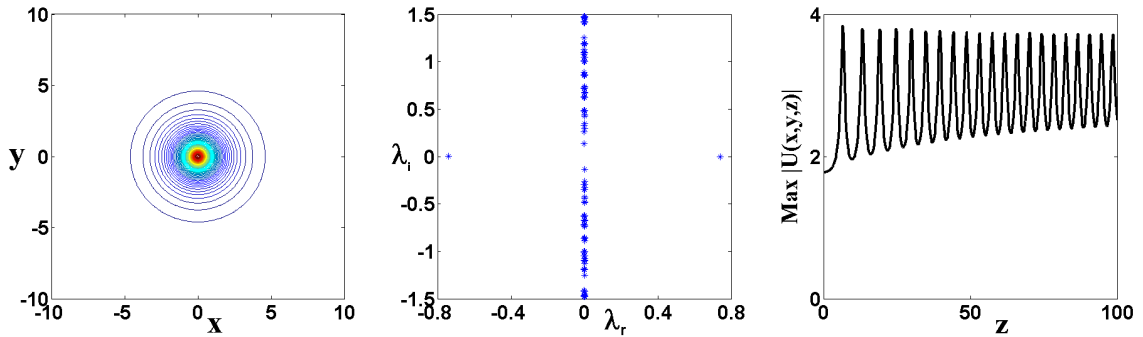


FIG. 11: (Color online) An example of an unstable 2D soliton in the single-well model, based on Eq. (40) with $\sigma = 0.02$ (the first panel). The propagation constant and total power of the soliton are $\mu = 0.25$ and $N = 5.2517$. The second panel shows the linear spectrum of small perturbations around the soliton. The third panel illustrates the transformation of the unstable soliton into a robust breather, which features regular oscillations of the amplitude.

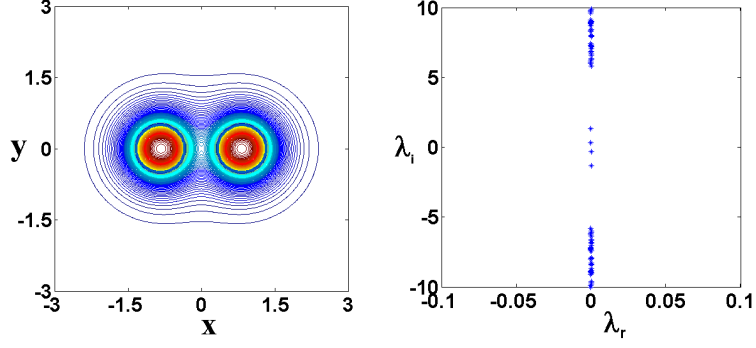


FIG. 12: (Color online) A stable symmetric double-peak soliton of equation (41) with $x_0 = 0.83$, $\sigma = 0.0288$ and $\mu = 5.76$, $N = 49.02$. Bold blue circles in the first panel and in similar figures below depict the shape of the regularization of the δ -functions per Eq. (42). Here and in similar figures below, the second panel shows the spectrum of stability eigenvalues for small perturbations around the soliton.

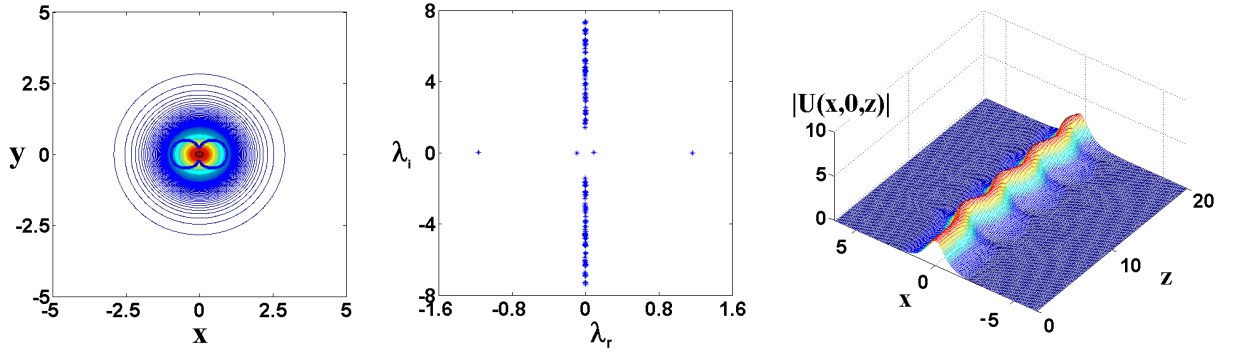


FIG. 13: (Color online) An unstable symmetric single-peak soliton of equation (41) with $x_0 = 0.45$, $\sigma = 0.0484$, and $\mu = 1.452$, $N = 6.1614$. Here and in similar figures below, the third panel shows the cross section $y = 0$ of the wave field in the course of its evolution.

particular, different branches are stable according to the VK or anti-VK criterion, depending on whether the SF or SDF term is the dominant one. Collapse of 2D modes never occurs in the presence of $\sigma > 0$.

The bifurcation loop accounting for the breaking and restoration of the symmetry is concave for the weak coupling between the circles ($x_0 = 0.83$), in Fig. 20, and convex for the strongly coupled (partly overlapping) circles, with $x_0 = 0.45$ in Fig. 22. This observation agrees with what was found before in the above-mentioned dual-core systems carrying the competing SF-SDF cubic-quintic nonlinearity [34]. Note that the concave and convex bifurcation loops

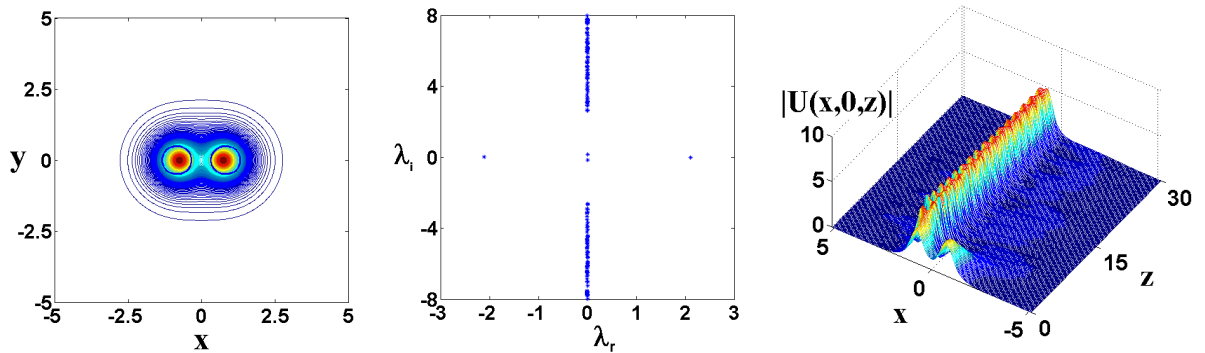


FIG. 14: (Color online) An unstable symmetric double-peak soliton of Eq. (41) with $x_0 = 0.83$, $\sigma = 0.0288$, and $\mu = 2.88$, $N = 11.95$.

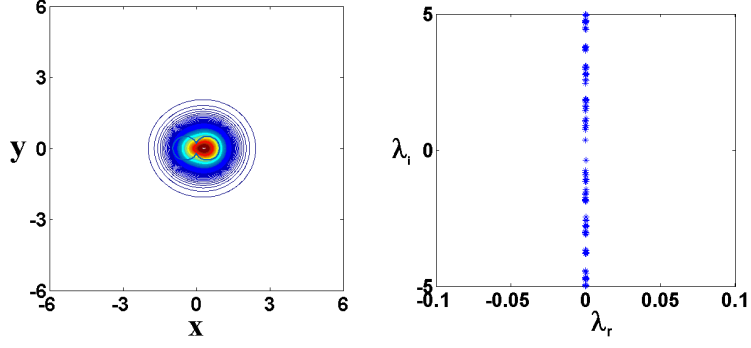


FIG. 15: (Color online) A stable asymmetric soliton of Eq. (41) with $x_0 = 0.45$, $\sigma = 0.0484$, and $\mu = 3.267$, $N = 17.246$, the asymmetry parameter being $\nu = 0.474$.

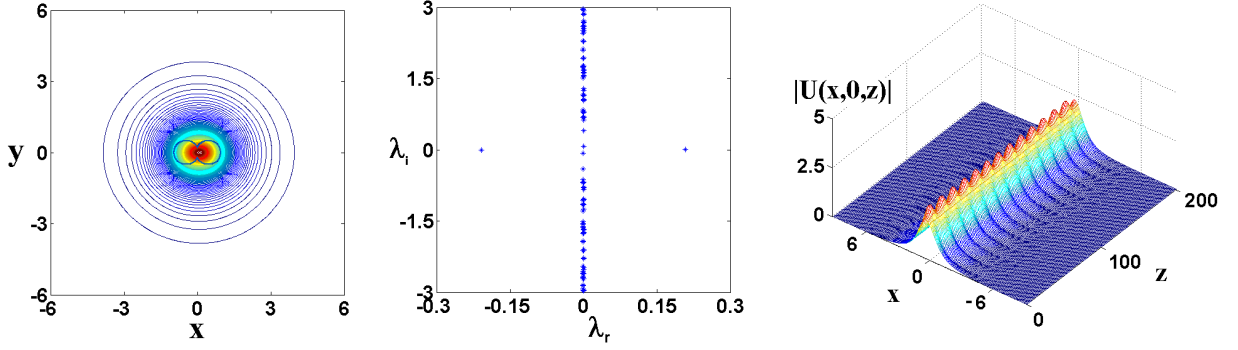


FIG. 16: (Color online) An unstable asymmetric soliton of Eq. (41) with $x_0 = 0.45$, $\sigma = 0.0484$ and $\mu = 0.557$, $N = 5.324$, the asymmetry parameter being $\nu = 0.131$.

correspond to strongly differing sets of the $N(\mu)$ curves, as seen from the comparison of Figs. 19 and 21.

V. CONCLUSIONS

The first objective of this work was to address the competition of SF and SDF (self-focusing and self-defocusing) nonlinearities in the system where both nonlinear terms have the same dimension (scaling behavior). The 1D system offers a physically relevant setting for the realization of such a system, in the form of the combination of the SF cubic term localized with the delta-functional coefficient, and the spatially uniform SDF quintic term. We have found, in the exact form, the most general family of the 1D Townes' solitons. It remains degenerate and unstable irrespective of

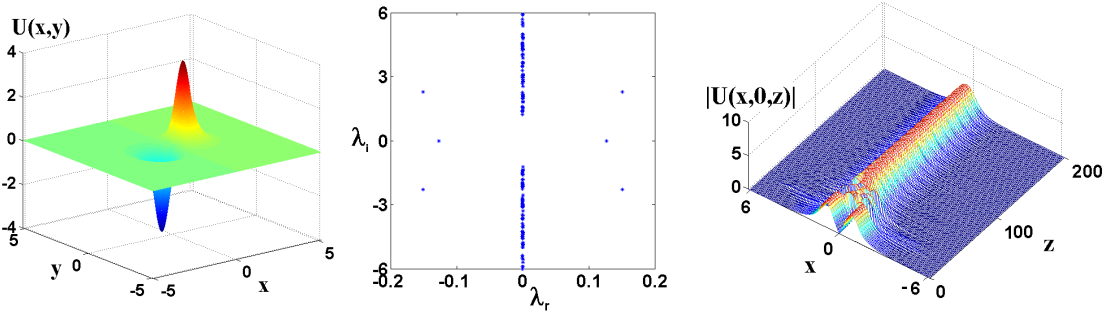


FIG. 17: (Color online) An unstable antisymmetric soliton of equation (41) with $x_0 = 0.45$, $\sigma = 0.0484$ and $\mu = 1.21$, $N = 13.7$.

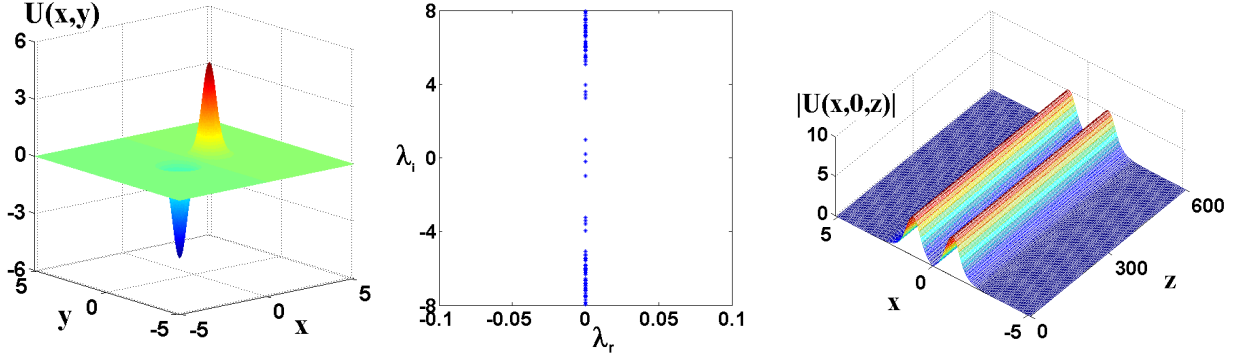


FIG. 18: (Color online) A stable antisymmetric soliton of Eq. (41) with $x_0 = 0.83$, $\sigma = 0.0288$ and $\mu = 5.04$, $N = 16.96$.

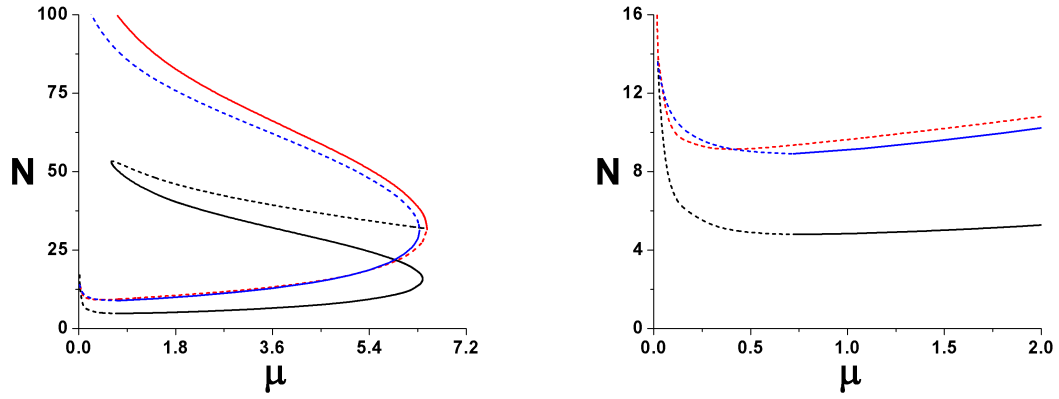


FIG. 19: (Color online) The first panel: the total power vs. the propagation constant, $N(\mu)$, for solitons in the 2D double-well system with $\sigma = 0.0288$ and $x_0 = 0.83$ [i.e., with non-overlapping circles in Eq. (41)]. The second panel is a closeup of a region at small μ of where the asymmetric branch splits off from the symmetric one. Here and below, the solid and dashed curves (or chains of symbols) represent, respectively, stable and unstable families of solitons. The red, blue, and black colors designate, severally, symmetric, antisymmetric, and asymmetric modes.

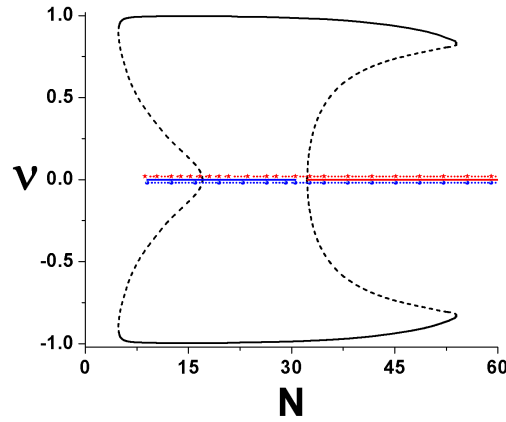


FIG. 20: (Color online) The symmetry-breaking diagram, $\nu(N)$, in the 2D double-well model (41) with $\sigma = 0.0288$ and $x_0 = 0.83$, i.e., non-overlapping circles.

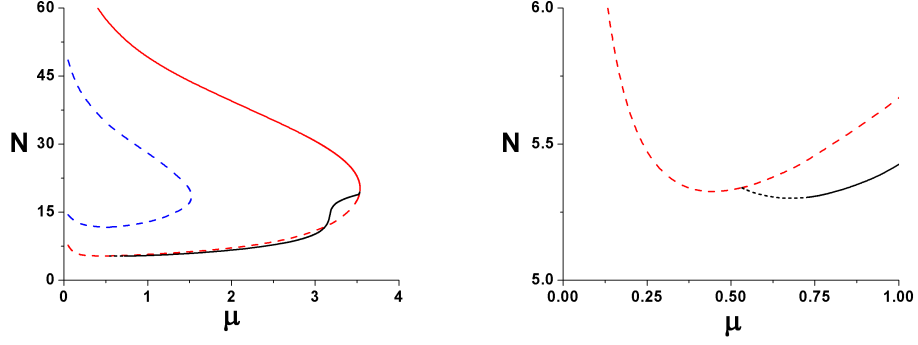


FIG. 21: (Color online) The first panel: the curves $N(\mu)$ for the 2D double-well system described by Eq. (41) with partly overlapping circles, $x_0 = 0.45$ and $\sigma = 0.0484$. The second panel is a closeup of the region of small μ , where the symmetry-breaking transition from symmetric to asymmetric solitons occurs.

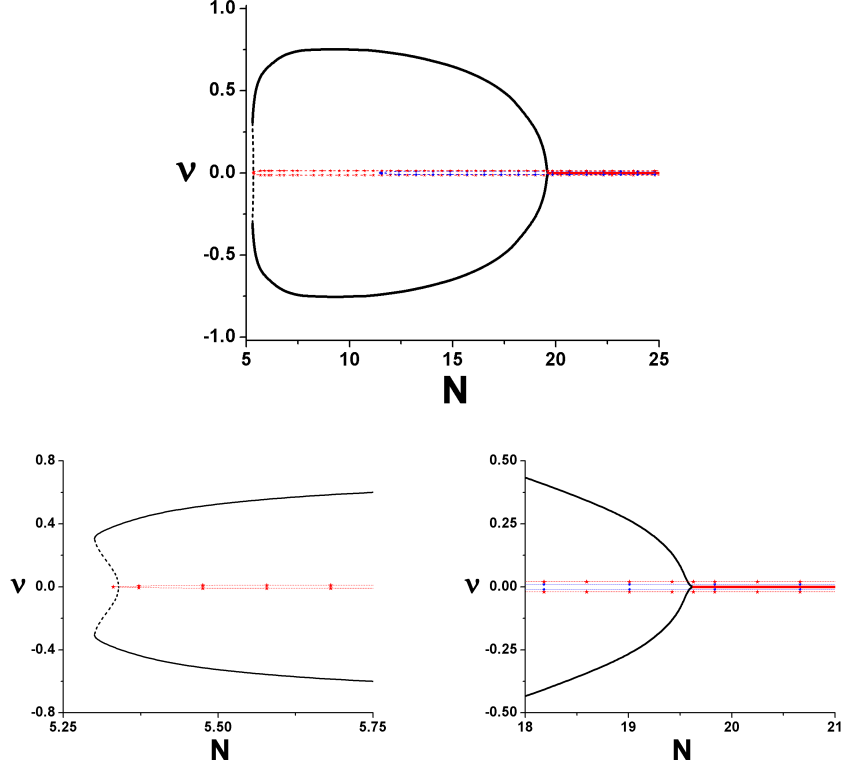


FIG. 22: (Color online) The symmetry-breaking diagram, $\nu(N)$ [the asymmetry measure, ν , is defined as per Eq. (44)] for the 2D double-well system, based on Eq. (41) with the partly overlapping circles, $x_0 = 0.45$, and $\sigma = 0.0484$. The two bottom panels are closeups of regions where the symmetry-breaking and restoring bifurcations (opening up and closing down of the bifurcation loop) take place.

the relative sign between the cubic and quintic terms. However, a weak regularization of the δ -function immediately stabilizes the solitons in the case of the competing (opposite) signs of the SF cubic and SDF quintic terms. These results were obtained, and mutually verified, in the numerical and analytical forms. Then, the analysis was extended to the 1D system with the pair of regularized δ -functions, and, eventually, to the 2D single- and double-delta-function systems. In all the cases, stable families of solitons have been identified.

In the 2D geometry, a remaining problem is to construct vortex solutions. A challenging possibility is to extend the analysis to 3D settings, which may be as physically relevant as the BEC model.

VI. ACKNOWLEDGEMENTS

This research is funded by Vietnam National Foundation for Science and Technology Development (NAFOSTED) under Grant number "103.01-2013.48" (N.V.H.).

-
- [1] S. Trillo and S. Wabnitz, *Opt. Lett.* **17**, 1572 (1992); M. A. Karpierz, *ibid.* **20**, 1677 (1995); S. Trillo, A. V. Buryak, and Y. S. Kivshar, *Opt. Commun.* **122**, 200 (1996); O. Bang, Y. S. Kivshar, A. V. Buryak, A. De Rossi, and S. Trillo, *Phys. Rev. E* **58**, 5057 (1998); T. J. Alexander, Y. S. Kivshar, A. V. Buryak, and R.A. Sammut, *ibid.* **61**, 2042 (2000); I. Towers, A. V. Buryak, R. A. Sammut, and B. A. Malomed, *ibid.* **63**, 055601(R) (2001).
 - [2] C. Etrich, F. Lederer, B. A. Malomed, T. Peschel, and U. Peschel, *Progr. Opt.* **41**, 483 (2000); A. V. Buryak, P. Di Trapani, D. V. Skryabin, and S. Trillo, *Phys. Rep.* **370**, 63 (2002).
 - [3] G. S. Agarwal and S. Dutta Gupta, *Phys. Rev. A* **38**, 5678 (1988); C. Zhan, D. Zhang, D. Zhu, D. Wang, Y. Li, D. Li, Z. Lu, L. Zhao, and Y. Nie, *J. Opt. Soc. Am. B* **19**, 369 (2002); R. A. Ganeev, M. Baba, M. Morita, A. I. Rysanyansky, M. Suzuki, M. Turu, H. Kuroda, *J. Opt. A: Pure Appl. Opt.* **6**, 282 (2004); K. Dolgaleva, R. W. Boyd, J. E. Sipe, *Phys. Rev. A* **76**, 063806 (2007).
 - [4] F. Smektala, C. Quemard, V. Couderc, and A. Barthélémy, *J. Non-Cryst. Solids* **274**, 232 (2000); G. Boudebs, S. Cherukulappurath, H. Leblond, J. Troles, F. Smektala, and F. Sanchez, *Opt. Commun.* **219**, 427 (2003); K. Ogusu, J. Yamasaki, S. Maeda, M. Kitao, and M. Minakata, *Opt. Lett.* **29**, 265 (2004); F. Sanchez, G. Boudebs, S. Cherukulappurath, H. Leblond, J. Troles, and F. Smektala, *J. Nonlin. Opt. Phys. Mater.* **13**, 7 (2004).
 - [5] B. Gu, Y. Wang, W. Ji, and J. Wang, *Appl. Phys. Lett.* **95**, 041114 (2009).
 - [6] E. L. Falcão-Filho, C. B. de Araújo, and J. J. Rodrigues Jr., *J. Opt. Soc. Am. B* **24**, 2948 (2007); E. L. Falcão-Filho, R. Barbosa-Silva, R. G. Sobral-Filho, A. M. Brito-Silva, A. Galembeck, and C. B. de Araújo, *Opt. Exp.* **18**, 21636 (2010); H. A. Garcia, G. B. Correia, R. J. de Oliveira, A. Galembeck, and C. B. de Araújo, *J. Opt. Soc. Am. B* **29**, 1613 (2012).
 - [7] E. L. Falcão-Filho, C. B. de Araújo, G. Boudebs, H. Leblond, and V. Skarka, *Phys. Rev. Lett.* **110**, 013901 (2013).
 - [8] S. Giorgini, L. P. Pitaevskii, and S. Stringari, *Rev. Mod. Phys.* **80**, 1215 (2008).
 - [9] P. F. Bedaque, E. Braaten, and H. W. Hammer, *Phys. Rev. Lett.* **85**, 908 (2000); E. Braaten, H. W. Hammer, and T. Mehen, *ibid.* **88**, 040401 (2002); M. W. Jack, *ibid.* **89**, 140402 (2002); F. Kh. Abdullaev, A. Gammal, L. Tomio, and T. Frederico, *Phys. Rev. A* **63**, 043604 (2001); W. Zhang, E. M. Wright, H. Pu, and P. Meystre, *ibid.* **68**, 023605 (2003); E. Fersino, G. Mussardo, and A. Trombettoni, *ibid.* **77**, 053608 (2008).
 - [10] C. Chin, R. Grimm, P. Julienne, and E. Tiesinga, *Rev. Mod. Phys.* **82**, 1225 (2010).
 - [11] D. Mihalache, D. Mazilu, L.-C. Crasovan, I. Towers, A. V. Buryak, B. A. Malomed, L. Torner, J. P. Torres, and F. Lederer, *Phys. Rev. Lett.* **88**, 073902 (2002).
 - [12] B. A. Malomed, D. Mihalache, F. Wise, and L. Torner, *J. Optics B: Quant. Semicl. Opt.* **7**, R53 (2005).
 - [13] L. Bergé, *Phys. Rep.* **303**, 259 (1998); E. A. Kuznetsov and F. Dias, *ibid.* **507**, 43 (2011).
 - [14] M. Quiroga-Teixeiro and H. Michinel, *J. Opt. Soc. Am. B* **14**, 2004 (1997); M. L. Quiroga-Teixeiro, A. Berntson, and H. Michinel, *J. Opt. Soc. Am. B* **16**, 1697 (1999); R. L. Pego and H. A. Warchall, *J. Nonlin. Sci.* **12**, 347 (2002).
 - [15] Yu. B. Gaididei, J. Schjodt-Eriksen, and P. L. Christiansen, *Phys. Rev. E* **60**, 4877 (1999); F. Kh. Abdullaev and M. Salerno, *Phys. Rev. A* **72**, 033617 (2005); G. L. Alfimov, V. V. Konotop, and P. Pacciani, *ibid.* **75**, 023624 (2007).
 - [16] D. E. Pelinovsky, Y. S. Kivshar and V. V. Afanasjev, *Physica D* **116**, 121 (1998).
 - [17] Kh. I. Pushkarov, D. I. Pushkarov, and I. V. Tomov, *Opt. Quantum Electron.* **11**, 471 (1979); S. Cowan, R. H. Enns, S. S. Rangnekar, and S. S. Sanghera, *Can. J. Phys.* **64**, 311 (1986).
 - [18] B. A. Malomed and M. Ya. Azbel, *Phys. Rev. B* **47**, 10402-10406 (1993).
 - [19] N. Dror and B. A. Malomed, *Phys. Rev. A* **83**, 033828 (2011).
 - [20] T. Mayteevarunyoo, B. A. Malomed, and G. Dong, *Phys. Rev. A* **78**, 053601 (2008).
 - [21] A. Acus, B. A. Malomed, and Y. Shnir, *Physica D* **241**, 987 (2012).
 - [22] J. Hukriede, D. Runde, and D. Kip, *J. Phys. D* **36**, R1 (2003).
 - [23] P. O. Fedichev, Yu. Kagan, G. V. Shlyapnikov, and J. T. M. Walraven, *Phys. Rev. Lett.* **77**, 2913 (1996); D. M. Bauer, M. Lettner, C. Vo, G. Rempe and S. Dürr, *Nature Phys.* **5**, 339 (2009); R. Yamazaki, S. Taie, S. Sugawa, and Y. Takahashi, *Phys. Rev. Lett.* **105**, 050405 (2010); M. Yan, B. J. DeSalvo, B. Ramachandhran, H. Pu, and T. C. Killian, *ibid.* **110**, 123201 (2013).
 - [24] M. Vakhitov and A. Kolokolov, *Radiophys. Quantum Electron.* **16**, 783 (1973).
 - [25] H. Sakaguchi and B. A. Malomed, *Phys. Rev. A* **81**, 013624 (2010).
 - [26] T. Mayteevarunyoo, B. A. Malomed, and A. Roeksabutr, *J. Mod. Opt.* **58**, 1977 (2011).
 - [27] I. M. Merhasin, B. V. Gisin, R. Driben, and B. A. Malomed, *Phys. Rev. E* **71**, 016613 (2005).
 - [28] Y. S. Kivshar and W. Królikowski, *Opt. Lett.* **20**, 1527 (1995).
 - [29] J. Yang, *J. Comp. Phys.* **227**, 6862-6876 (2008).
 - [30] J. Yang, *J. Comp. Phys.* **228**, 7007-7024 (2009).
 - [31] J. Yang, *Phys. Lett. A* **377**, 866 (2013).
 - [32] O. V. Borovkova, Y. V. Kartashov, B. A. Malomed, and L. Torner, *Opt. Lett.* **36**, 3088 (2011); R. Driben, Y. V. Kartashov, B. A. Malomed, T. Meier, and L. Torner, *Phys. Rev. Lett.* **112**, 020404 (2014).

- [33] A. Roeksabutr, T. Maytevarunyoo, and B. A. Malomed, *Opt. Exp.* **20**, 24559 (2012);
- [34] L. Albuch and B. A. Malomed, *Mathematics and Computers in Simulation* **74**, 312 (2007); Z. Birnbaum and B. A. Malomed, *Physica D* **237**, 3252 (2008).
- [35] H. Sakaguchi and B. A. Malomed, *Phys. Rev. E* **73**, 026601 (2006).